Holistic lithography for EUV: NXE:3100 characterization of first printed wafers using an advanced scanner model and scatterometry

Frank A. J. M. Driessen, N. Davydova, J. Jiang[a], H. Kang[b], V. Vaenkatesan, D. Oorschot, I.S. Kim[c], S.N. Kang[c], Y. Lee[c], J. Yeo[c], K. Gronlund[a], H.Y. Liu[a], K. van Ingen-Schenau, R. Peeters, C. Wagner, J. Zimmermann[d], O. Schumann[d]

ASML Netherlands B.V., De Run 6501, 5504 DR Veldhoven, The Netherlands
[a] ASML-Brion Technologies Incorporated, 4211 Burton Drive, Santa Clara, CA 95054, USA
[b] ASML Technology Development Center, 4211 Burton Drive, Santa Clara, CA 95054, USA
[c] Samsung Electronics, Co.,Ltd., San #16 Banwol-Dong, Hwasung-City, Gyeonggi-Do, Korea
[d] Carl Zeiss SMT GmbH, 73446 Oberkochen, Germany

ABSTRACT

In this paper we will present ASML's holistic approach to lithography for EUV. This total approach combines the various components needed to achieve the correct on-product demands of our customers in terms of patterning fidelity across the entire image field and across the entire wafer.

We will start giving a general update on ASML's NXE scanner platform of which the 6th NXE:3100 systems is now being shipped to a leading chipmaker. The emphasis will be on wafer imaging results for various applications such as flash memory and logic's SRAM. Then we will describe the second holistic component, NXE-computational lithography, which was developed to speed-up early learning on EUV and to achieve high accuracy on the wafers. Thirdly, the YieldStar angular-resolved scatterometry tool that supports the scanner's stability was used to characterize the system and calibrate the models.

The wafer-results reveal in detail predicted imaging effects of NXE lithography and allow a calibration of system parameters and characterization of hardware components. We will demonstrate mask-induced imaging effects and propose an improvement of the current EUV blank or mask-making processes.

Keywords: EUV, lithography, flare, NXE, scanner, reticle, photo-mask, CDU, imaging

1. INTRODUCTION

ASML's holistic lithography was introduced in 2009[1] for ArF-immersion lithography around the start of the 32-nm node. By integrating computational lithography, wafer lithography and process control, the industry's technology shrinks could be developed in a better way through co-optimization. For instance, with holistic lithography, manufacturing information and detailed models of the optics in the scanner are made available to the chip-design phase (for instance for source-mask optimization). Furthermore, lithography cluster and other process behavior can be stabilized in a better way.

In this paper we introduce and apply the concept of holistic lithography to EUV. Computational models have been developed that contain details of the newly introduced NXE scanner platform and of generic EUV effects such as those of EUV masks and the impact that flare has on each different mask layout. With these computational capabilities -which are available *before* the scanners are actually introduced to the field- ASML's customers will be capable of better understanding EUV lithography on *their* IC-devices and speed up their learning cycles in the semiconductor factories. The same holds for the mask-making industry: With the predictive computational tools the mask materials and process can be developed in a better way such as will be exemplified in this paper. The NXE scanners have a lot of metrology on board for system control and read out; however some of the metrology can be off-loaded to ASML's metrology tool YieldStar, which can either be positioned as a module integrated in a track, or stand-alone in the clean-room to control

Photomask Technology 2011, edited by Wilhelm Maurer, Frank E. Abboud,
Proc. of SPIE Vol. 8166, 81660Z · © 2011 SPIE · CCC code: 0277-786X/11/$18 · doi: 10.1117/12.898955

the full process in the former case, and multiple litho-clusters in the latter. This is of special importance during high-volume manufacturing (HVM). YieldStar is unique in that it is capable of measuring overlay, CD uniformity, resist thickness as well as focus (focus being under development in EUV) and it can interface with scanners through a product called BaseLiner to further stabilize the scanners. A schematic overview of the holistic lithography concept is shown in Figure 1. In the near future we will see further enhanced automation and data transfer between the three major components that form EUV holistic lithography.

In this paper we will describe the components of this total lithography approach and we will give examples how it was used to verify wafer results and compare them with predictions.

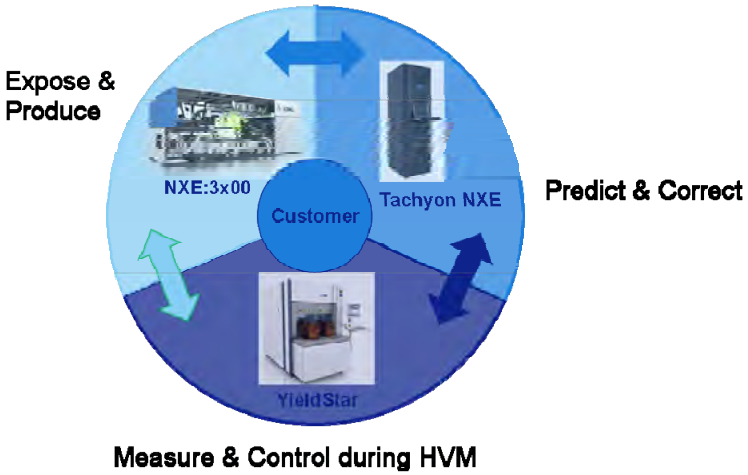

Figure 1: Schematic explaining holistic lithography for EUV: mutual interaction and integration of 1) NXE wafer exposure for production, with 2) computational lithography for prediction and (mask) correction, and 3) dedicated metrology for verification and control during high-volume manufacturing (HVM).

2. NXE SCANNER UPDATE

2.1 Scanner update

The NXE:3100 systems are ASML's first generation EUV scanners for the semiconductor factories; they transfer the learning of the two alpha-demo tools at IMEC and Albany to the industry. The NXE:3100 has been manufactured in a limited edition. The year 2011 truly marks the introduction of EUV scanners to the industry: six NXE:3100's have been transferred to customers. While writing this paper, three of them were exposing wafers, two of them were under installation and one was in final shipment phase.

The default illumination mode of the NXE:3100 has a numerical aperture (NA) of 0.25 and conventional illumination at $\sigma_{\_outer}$= 0.8. A selection of popular off-axis illumination (OAI) modes is possible as well albeit at the cost of a reduction of precious EUV light intensity. The NXE:3100 is intended to enable the 27-nm half-pitch node. An early performance validation has been reported by C. Wagner *et al.*[2]

The NXE platform is designed to support multiple technology nodes. The second generation scanner from this platform, the NXE:3300, will have an NA=0.33, a maximum $\sigma_{\_outer}$= 0.9, a selected set of loss-less OAI modes, and it intends to serve the industry down to 16-nm resolution. The NXE:3300 will also have again further-reduced flare values, higher source power, as well as a significantly lower footprint, which are all important factors for volume manufacturing.

2.2 Imaging results with the NXE:3100

This section summarizes imaging results for various CMOS device applications as obtained on the NXE:3100 at ASML premises. The NXE:3100 is specified for 27-nm node imaging but a lot of emphasis is given to extending its resolution.

Figure 2 shows SEM images for 22-nm node NAND flash wordline (WL) and contact-hole (CH) layers[3]. The process used was a 50-nm layer of SPURV002 photo-resist on 20nm under layer (UL). TBAH was used as developer and a DI-water rinse was used. Illumination used was dipole-X at 75-degree opening angle. Best doses used were 9.5 mJ/cm^2 for the line-space (L/S) mask and 13.0 mJ/cm^2 for the CH mask. The half-pitch for the WL mask was 22 nm and that for the CH mask was 24-nm. The corresponding process window for 22-nm 1:1 dense L/S under these conditions was measured to have 12% exposure latitude (EL) at 200-nm depth-of-focus (DOF); the Bossung curves associated to this are shown at the right of Figure 2.

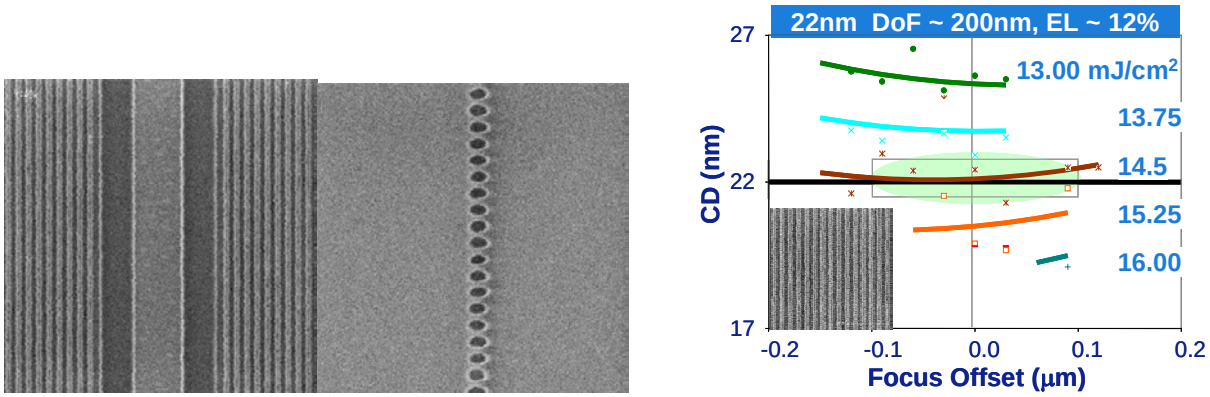

Figure 2: 22nm node Flash memory wordline at pitch 44 nm (left) and contact holes (middle) at CH pitch of 48-nm. Patterns were resolved on NXE:3100 using dipole-X illumination at 75-degree opening angle. Under these conditions the process window for 22-nm 1:1 dense L/S was 200-nm DOF at 12% exposure latitude as shown in the picture at the right for which an organic resist was used..

A staggered contact layer of pitch 65nm could also be well resolved as shown in Figure 3. Such staggered contacts are possibly part of the flash cells of the 18-nm node as indicated graphically in Figure 3 as well. The resist and developer process used was the same as described above with the exception that the DIW rinse was replaced by a FIRM[4] Extreme rinse. In Figure 3 also SEM images of 19 and 18-nm 1:1 dense L/S are shown, exposed using a 60-degree dipole illumination shape. At this squeeze of the resolution of NXE:3100 not much process window can be expected but it shows the imaging potential when going to the NXE:3300.

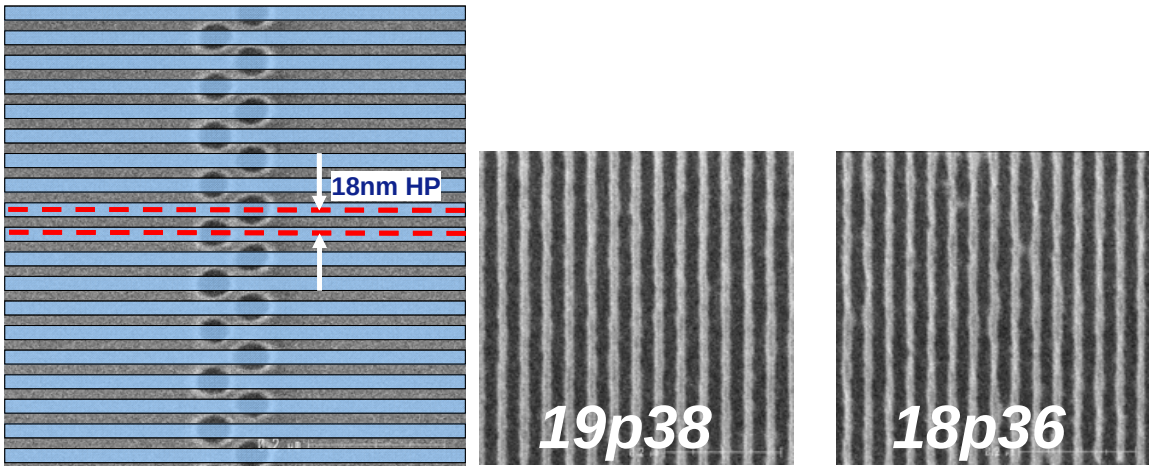

Figure 3: Left: The 18-nm node flash memory staggered contact layer is resolved. Bit-lines of 18-nm half-pitch have been projected on top of the SEM image for illustration purposes (Ref.[3]). Middle and right: 1:1 dense lines of 19 nm and 18 nm were printed, respectively using 60-degree dipole illumination in collaboration with IMEC using Inpria inorganic negative tone resist.

For logic and CPU applications the patterning capability of the SRAM is always a gating factor. In Figure 4 two mask layers of the 14-nm SRAM have been exposed; this SRAM has a bit cell size of 0.038 μm2. The left hand picture[2] shows the CH layer with half-pitch 30-nm and the right hand picture shows the metal-1 layer with half-pitch of 32-nm. Both masks are resolved well and obviously do need further optical-proximity correction (OPC) for all the details to print to target. Again the resist-process mentioned above with FIRM Extreme rinse was used.

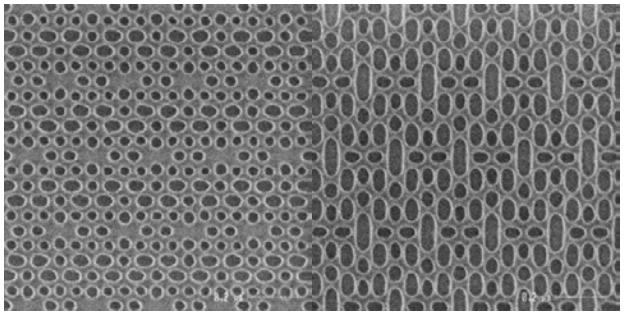

Figure 4: 14-nm node SRAM contact hole (left) and metal-1 layer (right) are well resolved on NXE:3100. Their half-pitches are 30 and 32 nm, respectively.

CD uniformity across the field is an important metric for manufacturing. Figure 5 shows CDU across the image field for 32-nm and 40-nm contact holes along with a CD-SEM image of the 32-nm dense holes. 3σ CD variation values of 1.8nm (left) and 1.4 nm (right) were achieved, respectively. A reticle-error correction was applied to the data.

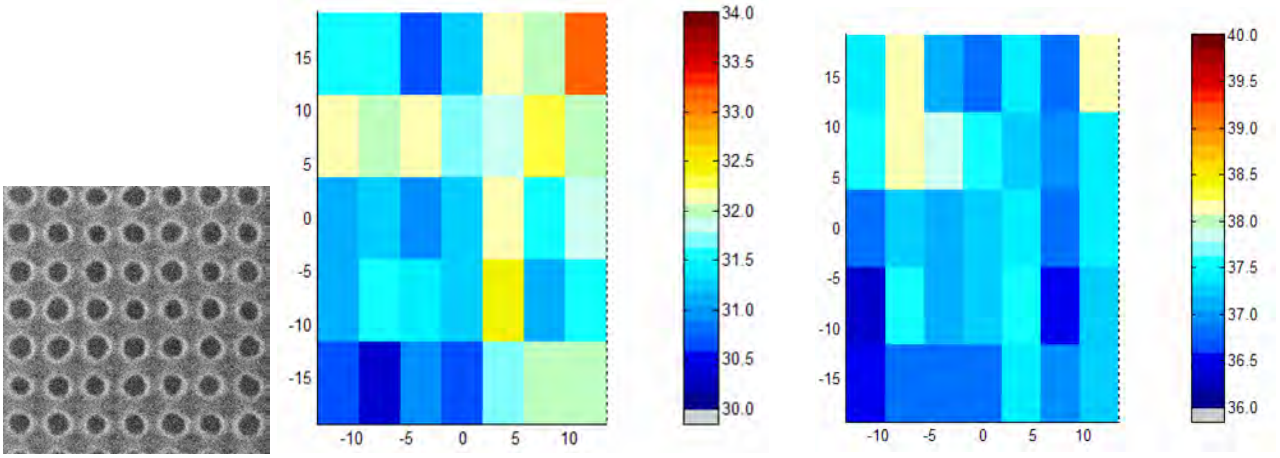

Figure 5: SEM Image of 32-nm dense contact holes (left), CD uniformity (representing 3sigma CD variation) across the image field was determined to be 1.8 nm for 32nm dense contact holes (middle) and of 1.4 nm for 40 nm dense contact holes (right); reticle error correction was applied.

3. COMPUTATIONAL LITHOGRAPHY UPDATE

The Tachyon NXE computational litho product was used during this work to compare the predicted imaging details of EUV lithography with measurements in order to calibrate parameters of the system. This Brion product supports the full NXE scanner characteristics along with generic EUV litho effects. In particular, flare effects induced by surface roughness of mirrors at the atomic level are obviously important in EUV[5,6] litho because of the short actinic wavelength of 13.5 nm. First, Tachyon NXE supports this generic flare with its long-range component described by the flare-point-spread function of the projection lens as measured after lens manufacturing. Furthermore, it also models the effects that certain scanner parts have on this flare before it reaches the wafer; all these effects then are included in the calculation of the mask-layout-specific flare-map used in OPC flows. Second, Tachyon takes the reflective mask properties and

material stack heights into account leading to shadowing effects that are a function of feature orientation and position on the mask[7]. Third, for proximity-effect compensation also details of scanner optics are modeled through slit such as 1) the details of the pupil shapes that contain discrete light spots (in contrast to the spatially continuous top-hat illumination in DUV lithography), 2) the behavior of pupils through slit, 3) other details of the projection lens such as the wavefront described by Zernikes. Numerous internal simulation studies were conducted to investigate the effects of the various scanner model components on 1 and 2-dimensional layout features. This was done both for NXE:3100 as well as for the upcoming NXE:3300. For the sake of brevity we can not report detailed results here but the general trends are that the benefits of including scanner imaging details increases for decreasing feature sizes and that they are more prominent for logic applications than for memory applications. Furthermore, including the effects of anisotropies in flare can improve the within-field CD control significantly up to 1nm. One final result we would like to show is the CD effect of the pupil details on printability of 2D layout pattern. This pupil consists of a collection of intensity spots, the intensity of which has small but predictable differences per spot that arise from the exact paths that the light travels inside the illuminator lens as well as from the details of the plasma. Because two types of sources of the plasma are available, LPP (laser-produced plasma) source and DPP (discharge produced plasma), minor effects on CD could be present. Figure 6 shows the CD difference that results when details of LPP and DPP are included in the pupil. The case used is the NXE:3300 scanner assuming 4% flare and a 7-nm resist blur for 22-nm features of interest. The RMS CD differences between LPP and DPP pupils through slit were found to be below 0.14 nm. Despite the fact that these effects are very small it is better to include the source details in the model to reduce their systematic CD impact.

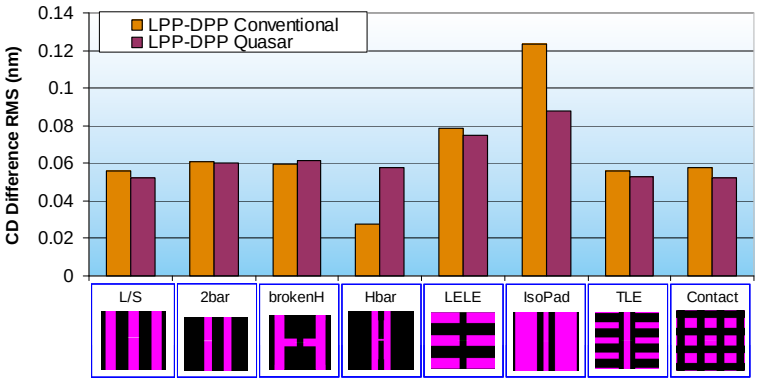

Figure 6: Differences in simulation results of CD's of various 2D pattern using either LPP or DPP as source pupils. This was done for two illumination modes, conventional and quasar for the case of the NXE:3300. Further explanation is given in the text.

4. EXPERIMENTAL CONDITIONS

4.1 Photomask

A special mask was designed by ASML to characterize imaging properties of the NXE scanner with emphasis on flare; furthermore it contains calibration structures for OPC. The design contains 30-nm dense line-space features to study 1) the flare point-spread function, 2) the symmetry of flare, 3) border-reflection effects, and 4) possible DUV reflections from the REMA-blade (a small fraction of DUV light is present in the source spectrum; its possible reflections should be well understood and controlled). The mask was manufactured at the captive mask shop of Samsung and reticle CD-uniformity data on it will be reported in the next section. Furthermore, multilayer reflectivity of 65% and absorber reflectivity of ~1% were measured at EUV wavelength of 13.5 nm by the mask shop. Finally, multilayer and absorber reflectance curves were available throughout the DUV-to-visible spectral region to ensure a proper analysis of effects.

4.2 Wafer exposures and metrology

Wafers were coated with a 50-nm thick photo-resist layer of Shin Etsu SPURV002. Nominal dose and focus settings were determined first from a FEM pathfinder wafer. The CD analysis of this wafer was done both by conventional Hitachi CD-SEM as well as by YieldStar[8]. Because of its excellent measurement accuracy (0.1nm details were resolved) and high speed (0.7 sec/measurement) YieldStar provided best value. We also used the YieldStar S100 to determine the

residual resist thickness after develop throughout the process window. YieldStar is furthermore capable of accurately measuring overlay effects but that was not part of this study. Wafer exposures were performed on two NXE:3100 scanners which both had laser-produced plasma (LPP) EUV sources. Conventional illumination was used with partial coherence of 0.8 at an NA of 0.25.

5. RESULTS AND DISCUSSION

5.1 Results on mask

The layout of the mask used to investigate the NXE is shown at the left of Figure 7. It contains dense metrology arrays such as A and B intended to characterize through-slit fingerprints and corner effects. The mask-CDU of the full array through slit measured by YieldStar is shown at the right of Figure 7. Very good CDU uniformity is observed of 0.8 nm (1σ). The two top corner arrays B even have a CDU of 0.5 and 0.6 nm. Pattern sequence C contains layout to measure the flare-PSF; the small pattern of dense lines in the center of them is embedded in large open areas of different shapes, a known tougher task to control for the etch step of the mask process. Nevertheless, the CDU of array C was still very good: 1.2 nm.

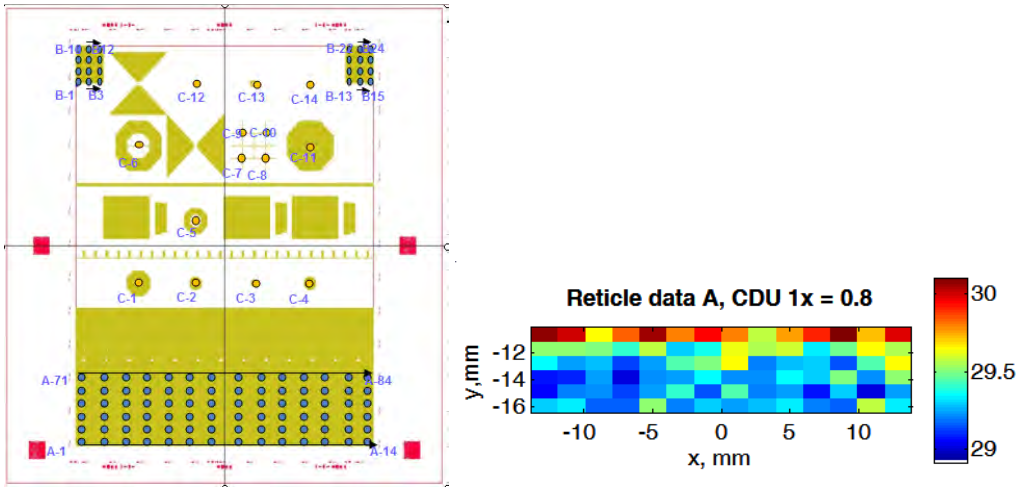

Figure 7: Layout of an ASML reticle for characterization of NXE scanner effects and mask CD measurements on 30-nm 1:1 dense line-spaces from the bottom array A-{1-84}. Further CDU results are given in the text.

5.2 Results on wafer

A pathfinder FEM wafer was used to determine best dose and focus conditions. Figure 8 shows the Bossung curves derived from the mean-CD-FEM readouts by YieldStar (left). At a dose of 14mJ/cm^2 an almost iso-focal behavior is observed. The YieldStar S-100 data also allowed us to extract the post-develop resist thickness values throughout the process window. Throughout the process window this thickness was fairly stable at ~40nm. This corresponds to a thickness-reduction of ~20% *cf.* the applied thickness of 50 nm.

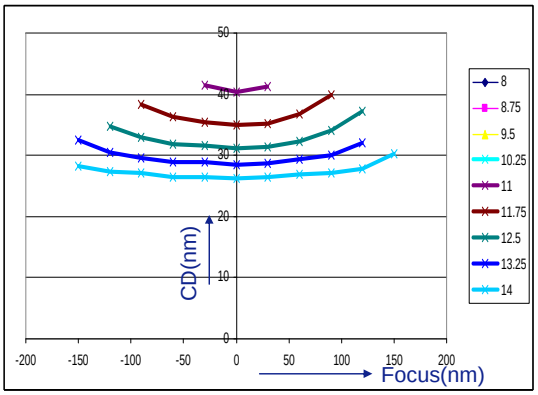

Figure 8: Bossung curves for best-focus, best-dose determination from YieldStar CD measurements with iso-focal plane achieved at ~14mJ/cm2 (left); resist-height throughout the process window was ~40nm.

Best dose and focus settings were then chosen to expose the wafers for the scanner imaging characterization. The wafer map used is shown in the in-set of Figure 9: both isolated fields (brown column in the center) as well as fields that have direct-neighbor fields exposed with zero-distance between the fields (field and image sizes of 26x32mm) are present on the wafer. The fields with neighbors can be separated in three different versions: fields with one, two and three neighbor exposures in the field corners, respectively.

Figure 9 shows across-wafer CD measurements of horizontal lines with flare light either coming from vertically (V) oriented butterfly structures or from horizontally (H) oriented ones. Note that because the measurement features are the same, there is no difference in shadowing effect that will influence the results. The horizontal axis corresponds to the field positions on the wafer. These measurements were taken by CD-SEM. The average CD in cases of H-flare is 33.7 ±0.7nm and that in case of V-flare is 33.6 ±0.6nm. Therefore, it can be concluded that for the NXE:3100 there is no flare difference caused by the orientation of the flare-generating open areas, which is indicative of the high isotropic quality of the mirror optics in the projection lens. As a matter of fact, if the 0.1nm difference would appear to be statistically significant, it could even be explained by the fact that the long-range flare at pattern V on the mask is slightly larger than that of pattern H on the mask. Flare map calculations by Brion indeed confirm this and predict a 0.1nm CD difference for the typical flare sensitivity of the resist used here.

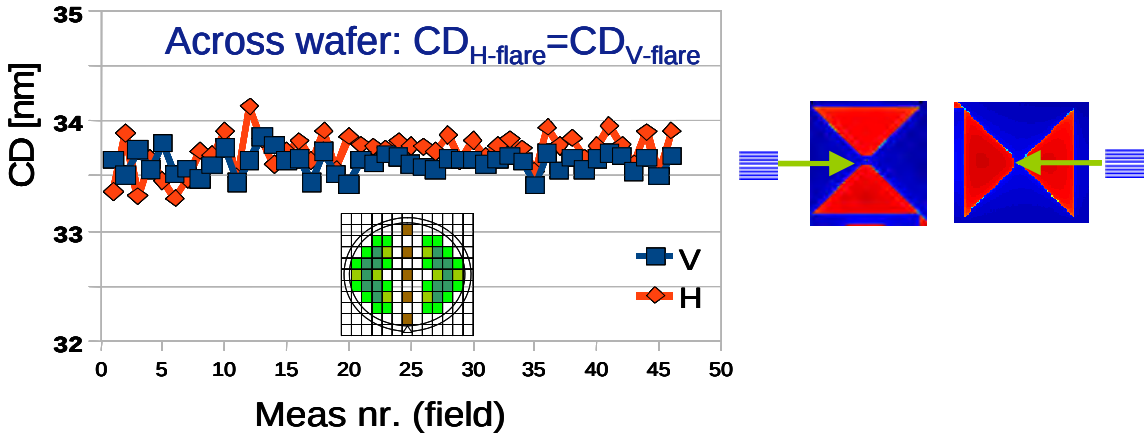

Figure 9: CD (nm) of horizontal lines measured across the wafer for flare originating from both vertical (V) butterfly structures and from horizontal (H) butterfly structures. The points on the horizontal axis correspond to the colored fields of the wafer map at the inset. No statistically significant CD difference is observed as a function of the different orientation of the flare-generating open areas.

Spectral control of the light is important in EUV lithography because the created EUV plasma generates also a small light intensity in the DUV part of the optical spectrum. For both the ADT as well as for the NXE:3100, the IMEC team showed that the DUV content in the light that reaches the wafer was already shown to be less than 1% [9]. That was concluded by investigating the direct reflections from the field with a special mask with Aluminum parts. Here, we will investigate possible reflection effects of DUV light. The only candidates in the scanner to exhibit DUV reflections are the REMA-blades. We investigated a scanner with old prototype REMA blades as well as a scanner with the real NXE:3100 REMA blades. The former proto blades were known to have high reflectivity in the DUV, whereas the latter production ones have low DUV reflectivity. The data in Figure 10 were achieved by subtracting the average CD field distribution of isolated fields from that of fields with neighbors. Furthermore, black-border reflection effects at the very edges of the fields were removed. The proto REMA blade case shows a residual CD fingerprint of maximum 0.8nm which is induced by a DUV reflection into the neighbor-field by the bottom REMA blade. The real NXE:3100 REMA does NOT show such characteristic fingerprint at all. This proves that DUV reflections are having no impact on production wafers with the NXE and that the REMA blades were well designed. Note that the CD color scale is the same for both plots. It may further be remarked that the metrology accuracy of these data achieved by YieldStar is extremely good: 0.1 nm CD differences are well resolved from it.

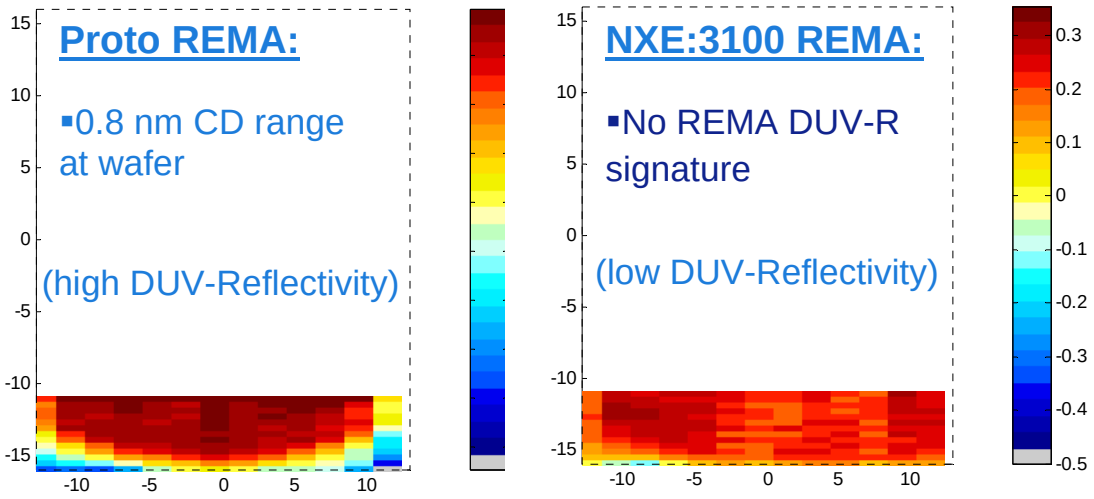

Figure 10: A prototype REMA shows a residual CD fingerprint arising from high reflectivity of residual DUV light in the lightsource (left); the production NXE:3100 REMA (with low DUV-R) shows absence of such fingerprint (right); CD color scales are identical for both plots.

Another important topic of interest in imaging with EUV photo masks stems from the fact that the mask-absorber stack does not (yet) have zero reflectance. This is not so much an issue for the dark features inside the field but it is of concern for the so-called black-border region (usually a ring-shaped border which optically isolates separate image-fields on a mask, and which also will capture the half-shadow (penumbra) in reflective lithography). Currently mask-black-border reflectivity values reported range from 0.5 to 2%: the thinner the absorber stack, the higher the reflectivity. Because of non-zero reflectivity of the black border (BB), EUV light can be reflected to the edges of the neighbor field. In field corners this can happen 2 or 3 times, depending on the number of neighbor fields.

In Figure 11 we show wafer YieldStar measurement again obtained by subtracting average CD values in isolated fields from those of densely packed fields. From left to right, one, two and three neighboring field exposures were present. The range of influence of this effect is typically a few 100 microns from the edge. In the presence of one neighbor field we observed a CD decrease of ~2.8nm at the field edges. In the field corners for the case of two and three neighbors, the CD decrease for L/S was ~5.2 and ~7.5nm, respectively. Especially in the corners this impact is large and we therefore urge mask makers to focus on mask process developments that further reduce the black-border reflectivity.

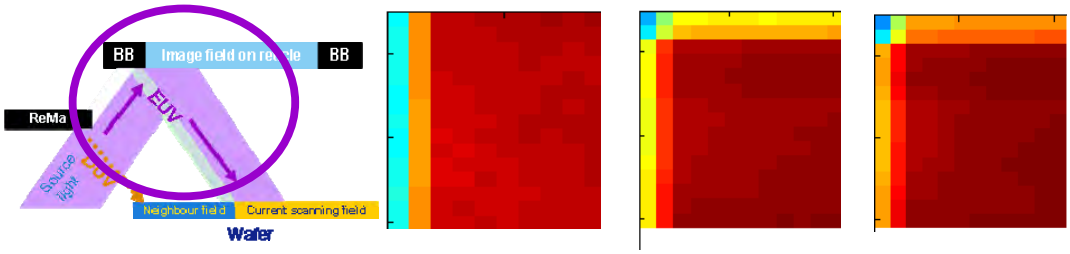

Figure 11: Effects on CD caused by mask-black-border reflections at the edges and corners of a field. Schematic at the left illustrating light reflection at the BB. The three colored pictures represent –from left to right- the measured CD's of 30-nm dense L/S in the top-left corner of the field in the presence of 1, 2 and 3 neighboring fields. At the edges of the field the CD decreases as a result of mask-BB reflection. Values are given in the text.

Tachyon NXE computational lithography can model the effects observed. In Figure 12 simulations and experimental results are compared head-to-head in a corner of the image field. For more detail on these simulations we refer to the work of N. Davydova et al.[10] at this conference. In Figure 15 of that paper, which at liberty is repeated here as the right graph of Figure 12, experimental and simulation data are shown along a cut-line for both horizontally and vertically oriented features. OPC will have a potential to correct for this effect but it will be preferential if the size of the BB effect is reduced by reducing the BB reflectivity.

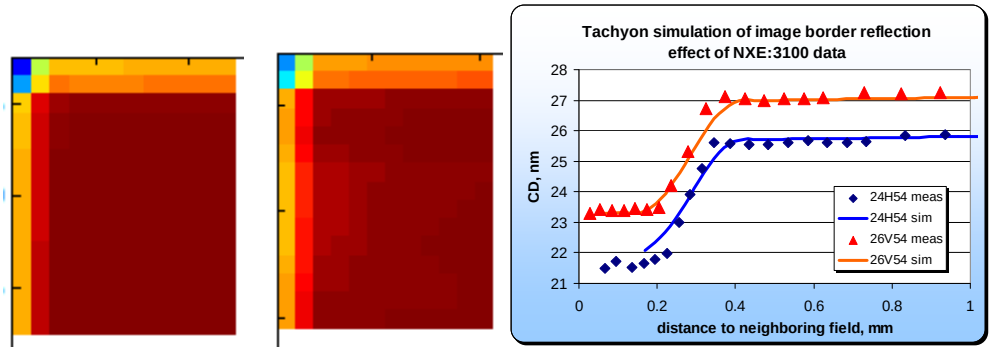

Figure 12: Simulation vs. wafer measurement match excellently: (left) Tachyon NXE simulation of mask-black-border effect for the CD features and the mask used in this experiment in the corner of the image field; (middle) YieldStar CD measurement of mask black-border effect. The right graph is from N. Davydova et al.[Ref.10] showing matching between simulation and her wafer-experiment for both horizontal and vertical features.

We would like to conclude this chapter by presenting good, independent model validation results on wafer flare as measured by IMEC and compare them with simulated flare maps by Brion's Tachyon NXE. For both the early ADT tool and the NXE:3100 detailed flare measurements were taken with a differently designed mask; this was done in the scan direction. Figure 13 shows these results for both the ADT with its high flare as well as for the NXE:3100 with low flare. The method uses open-frame measurements (so a real production mask will show much lower flare numbers) and has measurement features located at the edge of the field where the flare variations are known to be largest. An excellent match was obtained between wafer measurements and the simulated values. Similarly good results were obtained in the slit direction.

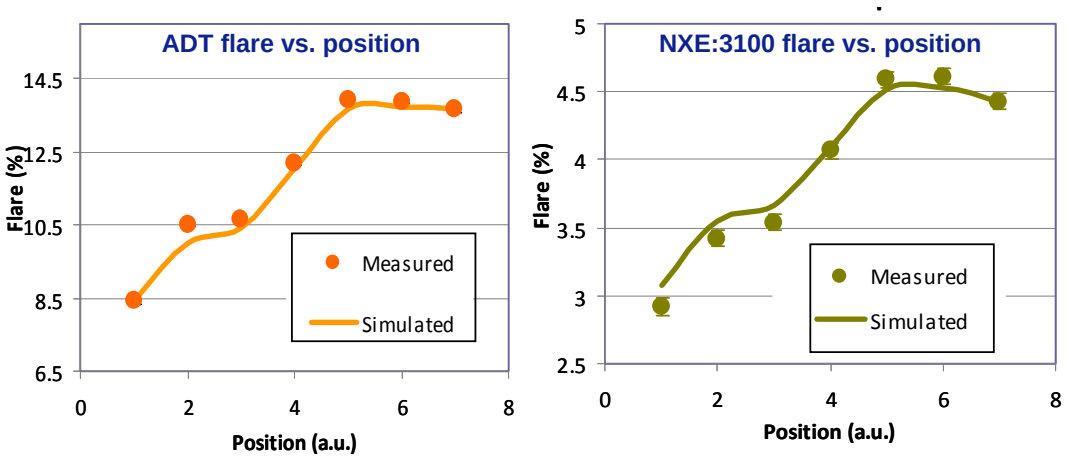

Figure 13: Measured flare data on wafer positions in the scan directions by IMEC (solid circles) vs. predicted flare values (simulated curves) at different positions on the mask. Validation was done for both the ADT as well as for the NXE:3100.

6. SUMMARY

We have introduced holistic lithography in EUV for the platform of NXE scanners: An integral approach that combines the capabilities of the NXE exposure tools with accurate predictive modeling and tailored metrology. We applied this concept to the first wafers exposed with the NXE:3100 scanners.

We gave a review of the status of the NXE scanner platform. With now six NXE:3100 scanner shipments to the field, the year 2011 can be marked as the year that EUV made its start to integration in the FABs. Extended imaging capabilities beyond the 27-nm targets were demonstrated for flash memory, logic-SRAM and dense contact hole applications with decent process windows for 22-nm and with imaging resolution down to 18-nm.

The imaging behavior of ASML's first prototype manufacturing platform NXE:3100 has been modeled in detail for computational lithography purposes. The model includes the optical system (pupil, slit, reflective projection lens), EUV-specific flare effects (extending from short to very long-range), the EUV mask properties, and other NXE:3100 hardware components. The accuracy of the model through the image-field was demonstrated by comparing it to wafer measurements. Accurate predictive modeling of the entire image-field is of high importance for ASML's customers to generate reliably (OPC) corrected and full-chip litho verified masks for a successful introduction of EUV to their FABs, thereby reducing learning cycles.

We presented printed wafer results using a special mask that was designed by ASML and manufactured by Samsung's captive mask shop. The mask measurements showed excellent uniformity and quality. The mask was designed to be able to characterize the specific flare details of EUV lithography such that parameters in the model could be extracted. Furthermore, the measurements yielded information on the quality of the projection optics in the NXE:3100.

The wafers were measured for CD uniformity by an ASML YieldStar S-100 scatterometry tool. After careful analysis of the large set of data, the results revealed predicted imaging effects of lithography such as flare details and residual black-border reflections from the mask absorber stack. Furthermore, it was shown that there was no wafer CD impact caused by out-of-band DUV reflections in the NXE:3100 scanners.

ACKNOWLEDGMENTS

The teams of Samsung Memory and Samsung Maskshop are greatly acknowledged for their support. Gian Lorusso of IMEC is acknowledged for his cooperation on flare and permission to show the measurement data in figure 13. Fruitful interaction with ASML's Eelco van Setten, Stuart Young, Hans Meiling, Noreen Harned and Jos Maas is greatly acknowledged. Finally, we want to thank Martin Lowisch, Martin Endres and Michael Patra of Carl Zeiss for their important contributions to modeling.

REFERENCES

[1] B. Koek, J. Koonmen, "ASML Introduces Holistic Lithography solutions to Continue Moore's Law", at SEMICON West, Press Release, see www.asml.com (2009).

[2] C. Wagner, J. Bacelar, N. Harned, E. Loopstra, S. Hendriks, I. De Jong, P Kuerz, L. Levasier, M van de Kerkhof, M. Lowisch, H. Meiling, D. Ockwell, R. Peeters, E. Van Setten, J. Stoeldraijer, S. Young, J. Zimmerman, Ron Kool, "EUV Lithography at Chipmakers has started: Performance Validation of ASML's NXE:3100", Proc. SPIE 7969, 79691F-1 (2011).

[3] J. Miyazaki, "EUV lithography into production at chipmakers: update on ASML's NXE platform", 7th Annual SEMATECH Symposium Japan, (2011).

[4] K. Petrillo, G. Huang, D. Ashworth, J. Georger, L. Ren, K. Y. Cho, W. Montgomery, S. Wurm, S. Kawakami, S. Dunn, and A. Ko, "Line width roughness control and pattern collapse solutions for EUV patterning", Proc. SPIE 7969, 796913 (2011).

[5] G.F. Lorusso, A.M. Goethals, R. Jonckheere, J. Hermans, K. Ronse, A.M. Meyers, I. Kim, A. Niroomand, F. Iwamoto, and D. Ritter, "Extreme ultraviolet lithography at IMEC: Shadowing compensation and flare mitigation strategy", Proc. SPIE 7969, 79692O-1 (2011).

[6] H. Aoyama, Y. Tanaka, T. Kamo, N. Iriki, Y. Arisawa, and T. Tanaka, "Flare evaluation for 32-nm half pitch using SFET", Proc. SPIE 6921, 69213H (2009).

[7] C. W. Ng, Kuen-Yu Tsai, Yen-Min Lee, Fu-Min Wang, Jia-Han Li, and Alek C. Chen, "Fully model-based methodology for simultaneous correction of extreme ultraviolet mask shadowing and proximity effects", J. Micro/Nanolith. MEMS MOEMS 10, 013004 (2011).

[8] J. Maas, M. Ebert, K. Bhattacharyya, H. Cramer, A. Becht, S. Keij, R. Plug, A. Fuchs, M. Kubis, T. Hoogenboom, and V. Vaenkatesan, "YieldStar: a new metrology platform for advanced lithography control", Proc. SPIE 7985, 79850H (2011).

[9] G. F. Lorusso, N. Davydova, M. Eurlings, C. Kaya, Y. Peng, K. Feenstra, T. H. Fedynyshyn, O. Natt, P. Huber, C. Zaczek, S. Young, P. Graeupner, and E. Hendrickx, “Deep ultraviolet out-of-band contribution in extreme ultraviolet lithography: predictions and experiments”, Proc. SPIE 7969, 79692O (2011).

[10] N. Davydova, E. van Setten, S-I Han, M. van de Kerkhof, R. de Kruif, D. Oorschot, J. Zimmerman, A. Lammers, B. Connolly, F. Driessen, A. van Oosten, M. Dusa, Y. van Dommelen, N. Harned, J. Jiang, W. Liu, H. Kang, H. Liu, “Mask aspects of EUVL imaging at 27nm node and below”, Proc. SPIE 8166-67 (2011).